Chinese Chemical Letters 37 (2026) 111490

Contents lists available at ScienceDirect

Chinese Chemical Letters

journal homepage: www.elsevier.com/locate/cclet

Characterization of intrinsic defects and their effects on carrier lifetime in CdTeSe: First principles and non-adiabatic molecular dynamics simulations

Hongqin Chu[a], Liyang Li[a], Fan Yang[a], Shujuan Li[b], Jiayao Wang[b], Shulai Lei[b,c,*], Jinbo Sun[b], Ke Xu[b], Xinyue Xiong[b], Zhenpeng Hu[a,*]

[a] School of Physics, Nankai University, Tianjin 300071, China
[b] School of Physics and Electronic Engineering, Hubei Key Laboratory of Low Dimensional Optoelectronic Materials and Devices, Hubei University of Arts and Science, Xiangyang 441053, China
[c] Hubei Longzhong Laboratory, Xiangyang 441053, China

ARTICLE INFO

Article history:
Received 14 March 2025
Revised 16 June 2025
Accepted 18 June 2025
Available online 20 June 2025

Keywords:
First-principles calculation
Intrinsic defects
Non-adiabatic molecular dynamics
Electron-hole recombination
Non-adiabatic coupling

ABSTRACT

With the rapid advancement of solar cell and radiation detector technology, understanding and controlling intrinsic defects in semiconductor materials is crucial for improving photovoltaic device performance. This study employs density functional theory (DFT) and non-adiabatic molecular dynamics (NAMD) methods to investigate the ground-state properties of intrinsic defects in CdTeSe (CTS) material and their impact on carrier dynamics. The results demonstrate that defect formation is strongly influenced by the chemical environment: acceptor defects are favored in Te-rich conditions, donor defects are promoted in Cd-rich conditions, while Se substitution at the Te site (Se_{Te}) and Te substitution at the Se site (Te_{Se}) defects are readily formed under various conditions due to their low formation energies. Carrier lifetime is significantly affected by various defects, as shown by their modulation of electron-phonon coupling interactions in electron-hole recombination dynamics. Se_{Cd} and Te_{Cd} defects are characterized by strong coupling between local vibrational modes and band-edge states, which enhances non-adiabatic coupling (NAC) strength and reduces recombination times to 9.44 ns and 30.95 ns, respectively. In contrast, Se_{Te} and Te_{Se} defects suppress the NAC by markedly reducing coupling, thereby extending the recombination times to 198.04 ns and 239.5 ns. Fourier transform analysis further indicates that the low-frequency phonon modes associated with Se_{Te} and Te_{Se} defects enhance carrier dynamics by optimizing phonon-assisted processes. Finally, it is found that variations in carrier concentration have a significant impact on carrier recombination, especially at high non-equilibrium carrier concentrations, which notably shorten the carrier lifetime. This study offers a theoretical framework for the performance optimization and defect engineering of CTS material in high-efficiency solar cell applications.

© 2026 Published by Elsevier B.V. on behalf of Chinese Chemical Society and Institute of Materia Medica, Chinese Academy of Medical Sciences.

With the global demand for renewable energy and efficient detection technologies, CdTeSe (CTS) is attracting growing attention for its unique physical and chemical properties, positioning it as a crucial material for research in solar cells and radiation detectors [1]. Compared to pure CdTe, selenium (Se) incorporation significantly enhances performance, particularly in crystal quality, bandgap tuning, and carrier transport. The selenium segregation coefficient is near unity, which facilitates the maintenance of a highly uniform composition distribution during the CTS crystal growth process, reduces compositional gradients and impurity accumulation, thereby enhances the long-term stability of the device [2,3]. In radiation detectors, Se promotes solid solution hardening, significantly reducing subgrain boundary networks [4,5]. Roy *et al.* found that the concentration of Te inclusions and precipitates in CTS is 5–8 times lower than that in CdZnTe (CZT) [6]. Additionally, the etch pit density of CTS crystals is an order of magnitude lower than that of CZT crystals, with reduced dislocation density offering a significant advantage for CTS as a substrate [7]. In solar cell applications, the incorporation of CTS layers significantly enhances cell efficiency [8]. Fiederle *et al.* observed that CTS crystals with 10% Se concentration, grown by the Bridgman method, displayed an electron $\mu\tau$ product (4.2×10^{-2} cm^2/V), superior to that of $Cd_{0.9}Zn_{0.1}Te$ [9]. Similarly, Kim *et al.* found that CTS sam-

* Corresponding authors.
E-mail addresses: sllei@hbuas.edu.cn (S. Lei), zphu@nankai.edu.cn (Z. Hu).

https://doi.org/10.1016/j.cclet.2025.111490
1001-8417/© 2026 Published by Elsevier B.V. on behalf of Chinese Chemical Society and Institute of Materia Medica, Chinese Academy of Medical Sciences.

ples grown by the same method achieved an electron $\mu\tau$ product of 6×10^{-4} cm^2/V, highlighting their superior performance in carrier transport [3]. Se inclusion reduces the bandgap, decreases its effective mass, and increases the photocurrent of the solar cell, while maintaining a high open-circuit voltage (V_{oc}), thus offering the potential to improve photovoltaic efficiency without sacrificing performance [10].

Despite the high compositional uniformity of CTS, point defects may still form during growth [11]. Due to the atomic radii's difference between Te and Se, Se atom distribution may be uneven, resulting in the formation of solute vacancies, substitutional defects, or interstitial atoms. These defects cause local lattice distortion, modify the bandgap, and affect carrier mobility and lifetime, thereby affecting electronic properties [12]. Specifically, the Cd vacancy (V_{Cd}) in CTS typically forms deep traps in the bandgap, promoting non-radiative recombination, leading to decreased carrier lifetime and limiting device performance [13]. Therefore, investigating the impact of point defects on CTS crystal properties is essential for optimizing growth and improving application performance.

While current experimental methods, such as admittance spectroscopy, deep level transient spectroscopy (DLTS), and white beam X-ray diffraction topography (WBXDT), have made significant progress in defect identification and characterization [12,14,15], challenges still exist in analyzing the microscopic behavior of defects. Specifically, the dynamic observation of individual defects is often hindered by experimental conditions, particularly under varying temperature, chemical potential, and electric field conditions, making it difficult to fully simulate their effects on electronic structure. First-principles calculations are widely used to study point defect behavior [16–20], as they predict the formation energy, stability, and energy level characteristics of defects at the atomic scale [21–23]. Additionally, the role of defects in non-radiative process can be revealed through non-adiabatic molecular dynamics (NAMD) methods [24,25], offering deeper insight into their impact on carrier lifetime and optoelectronic performance [26–29].

This study systematically reveals the intrinsic defect characteristics in CTS materials, including three vacancy defects (V_{Cd}, V_{Te} and V_{Se}), three interstitial defects (Cd_i, Te_i and Se_i) and six antisite defects (Cd_{Te}, Cd_{Se}, Te_{Cd}, Te_{Se}, Se_{Cd} and Se_{Te}). Employing density functional theory (DFT) calculations, we analyze the defect formation energies and their transition energy level variations in Cd-rich and Te-rich environments, clarifying the critical role of these defects in band structure modulation. Furthermore, relying on the NAMD methods, this study further explores the impact mechanism of defect-induced bandgap tuning on carrier recombination dynamics. It is shown that CTS exhibits a long carrier lifetime, and the presence of Se_{Te} and Te_{Se} defects further enhances this characteristic by slowing the carrier recombination rate. Finally, the influence of carrier concentration on the CTS carrier lifetime is further investigated, with particular emphasis on its pivotal role in modulating the electrical transport properties of materials. By analyzing the defect mechanisms in CTS materials, this study establishes a theoretical foundation for further research on their application in optoelectronic devices.

In this study, multiple possible charge states are systematically considered in the calculation of defect formation energies and transition levels, allowing the thermodynamic stability and ionization behavior of intrinsic defects to be comprehensively characterized under varying Fermi level conditions [30,31]. The methodology enables the identification of dominant charge transition paths and defect level positions, and it is widely used in semiconductor defect physics as a standard framework for evaluating thermodynamic defect behavior. The neutral charge state ($q=0$) is used as the foundational model in subsequent analyses of electronic structure and non-radiative carrier dynamics. An electronically saturated ground state is typically represented by the neutral configuration, which features well-defined local lattice relaxations and vibrational characteristics, making it ideal for identifying phonon modes and quantifying electron–phonon interactions. Moreover, under conditions of thermal equilibrium or low excitation, defects are generally found to reside in neutral or nearly neutral charge states [28,32]. The use of this approach is widely accepted in literature, as it offers both physical relevance and computational feasibility.

Based on DFT, this study performs first-principle calculations using the VASP software [16,17]. The HSE06 hybrid functional is applied to describe defect state energies and electronic structures [33]. By introducing the Hartree-Fock exchange term, this functional overcomes the limitations of the traditional generalized gradient approximation (GGA) in describing band gaps and strongly correlated electron systems [34]. And for reducing the computational cost, the Perdew-Burke-Ernzerhof (PBE) functional is used in first-principles molecular dynamics (MD) simulations. The Projector Augmented Wave (PAW) method is employed to describe electron-ion interactions [35]. The plane wave kinetic energy cutoff is set to 400 eV, and all the structures are fully relaxed until the total energy and forces on each atom are smaller than 10^{-5} eV and 0.02 eV/Å, respectively. In the study of CTS, we focused on the composition $CdTe_{0.875}Se_{0.125}$, as the cubic phase of $CdTe_{1-x}Se_x$ is stable within the range [36]. A 256-atom orthogonal supercell is constructed to investigate the impact of a single defect on the material properties. Defects are introduced by periodically repeating the original unit cell, which avoids interference from periodic effects and guarantees that the defect independently influences the electronic structure and mechanical properties [37]. K-point sampling is performed using only a single Γ point, which is appropriate for systems with strong periodicity or materials with large unit cells.

Our research employs advanced first-principles NAMD to investigate the impact of intrinsic defects on carrier recombination dynamics in CTS. After the geometry optimization, the systems are heated to 300 K for 5 ps in the canonical ensemble. A 5 ps first-principles MD simulation is then carried out with a 1 fs time step in a microcanonical ensemble. Carrier recombination dynamics are simulated using the Hefei-NAMD program [38,39], which is based on the quantum-classical decoherence surface hopping (DISH) method [40]. In long-timescale simulations, the final 3 ps of the MD trajectory are repeated multiple times to more thoroughly investigate the long-term evolution of dynamics. We sample 50 different initial configurations and 500 surface-hopping trajectories for each initial structure.

The electrical properties of CTS are derived from the band structure and DOS analysis, as shown in Fig. 1. The calculation results show that the direct bandgap of CTS at the Γ point is 1.54 eV, which is consistent with the experimental value for CTS samples with 10 % Se reported in the literature [41]. The energy states near the Fermi level are primarily dominated by contributions from Te and Se atoms. Te atoms contribute significantly to the density of states in the valence band, especially near the valence band maximum (VBM). Se atoms show a distinct electronic state distribution near the Fermi level, especially at the VBM and the conduction band minimum (CBM), reflecting the modulation of the electronic structure by Se doping. In contrast, Cd atoms are primarily located far from the Fermi level, showing minimal contribution to the band edges, while exerting a greater impact on deeper electronic states.

The intrinsic point defects in CTS are systematically investigated, covering all possible defect types. The transition energies for these defects are calculated and presented in Fig. 2a. V_{Cd}, Te_{Cd}, Te_i, Se_i, Se_{Cd}, Te_{Se} and Se_{Te} are classified as acceptor-type defects. V_{Cd} is a shallow acceptor, with its $V_{Cd}^{2-} \rightarrow V_{Cd}^{-}$ and $V_{Cd}^{-} \rightarrow V_{Cd}^{0}$ transi-

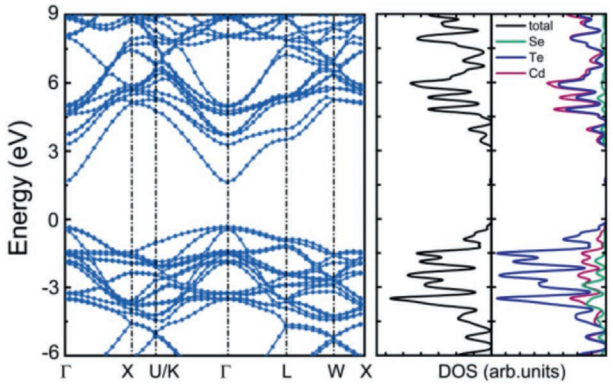


Fig. 1. Band structure, total density of states (DOS), and partial DOS of CTS material. The blue, green, and magenta curves represent the DOS of Te, Se, and Cd, respectively. Calculations are performed using the HSE06 hybrid functional.

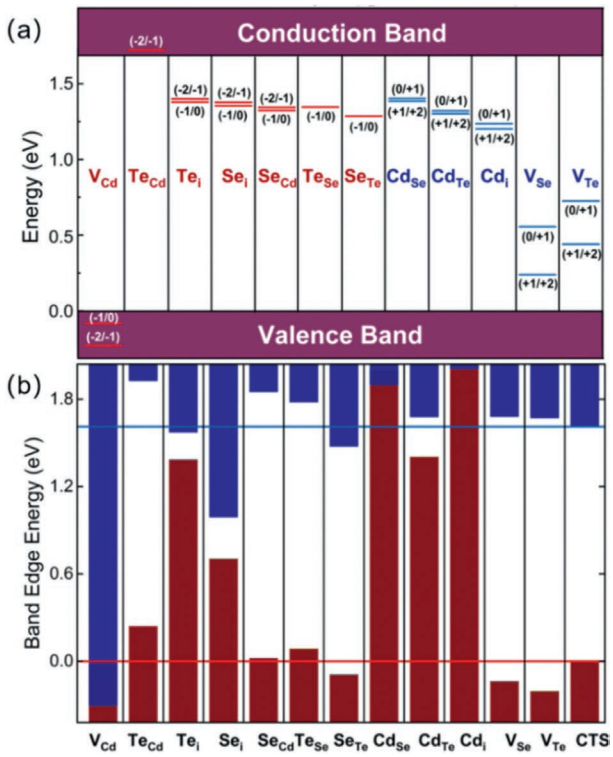


Fig. 2. (a) The transition energy levels of intrinsic point defects in the band gap of CTS. Red bars represent acceptor levels, and blue bars represent donor levels. The charge transitions are indicated in parentheses as (q/q'), corresponding to transitions from charge state q to q'. These charge states are consistent with those described in the text using Kröger-Vink-like notation (*e.g.*, $V_{Cd}^{-} \rightarrow V_{Cd}^{0}$). (b) The calculated occupied and unoccupied states shift caused by intrinsic defects in CTS. The red and blue lines show the valence and conduction band positions of CTS, respectively.

tion energy levels positioned 0.1 eV and 0.2 eV below the VBM, respectively. These energy levels are situated near the VBM and possess a negative charge, which facilitates electron acceptance and hole formation, thus enhancing p-type conductivity. In contrast, the acceptor transition levels of Te_{Cd} and Te_i are located below the conduction band, with their $Te_{Cd}^{2-} \rightarrow Te_{Cd}^{-}$, $Te_i^{2-} \rightarrow Te_i^{-}$, $Te_{Cd}^{-} \rightarrow Te_{Cd}^{0}$ and $Te_i^{-} \rightarrow Te_i^{0}$ transitions characterized as deep acceptor defects, which may capture electrons and consequently suppress conductivity. Donor characteristics are demonstrated by Cd_{Se}, Cd_{Te}, Cd_i, V_{Se} and V_{Te}. In particular, the (0/+1) and (+1/+2) transition levels of Cd_{Te}, Cd_i and Cd_{Se} are close to the CBM, classifying them as shallow donor defects. These shallow donor defects enhance n-type conductivity through their ability to readily release electrons. In contrast, the $V_{Se}^{0} \rightarrow V_{Se}^{+1} \rightarrow$ and $V_{Se}^{+1} \rightarrow V_{Se}^{+2}$ transition levels of V_{Se} are positioned at 0.7 eV and 0.8 eV from the CBM, indicating that it functions as a deep donor defect.

The modulatory effects of different intrinsic defects on the band-edge position of CTS are significant. All defect configurations are considered in their neutral charge states, which provide a consistent basis for evaluating band-edge modulation. As shown in Fig. 2b, acceptor-type defects, including V_{Cd}, Te_{Cd}, Te_i, Se_i, Se_{Cd}, Te_{Se}, and Se_{Te}, greatly influence the position of occupied states. They generally shift the highest occupied state upward, with the most pronounced increases caused by V_{Cd} and Te_{Cd}. The upward movement of the highest occupied state is attributed to the introduction of localized states, which reduce the binding energy of valence band electrons, narrowing the bandgap and facilitating the hole generation. Consequently, acceptor-type defects enhance p-type conductivity. In contrast, donor-type defects (Cd_{Se}, Cd_{Te}, Cd_i, V_{Se}, and V_{Te}) exert a more pronounced influence on unoccupied states. The defects typically cause the lowest unoccupied state to shift downward, with the shifts induced by Cd_{Te} and V_{Se} being particularly pronounced. Localized electronic states introduced by donor-type defects alter the energy level distribution near the CBM, which facilitates electron transition. The downward shift of the unoccupied states may reduce the threshold energy for electron excitation, increasing the number of free electrons and enhancing n-type conductivity.

In CTS, the formation energy of intrinsic defects is influenced by the variation in the Fermi level, revealing changes in defect charge states and the electronic structure in different chemical environments (Fig. 3). The formation energy of defects refers to the energy required to create defects in the material, and it is influenced by factors such as chemical potential, Fermi level, and chemical environment. Detailed calculations regarding defect formation energy, chemical potentials, and the influence of different chemical environments on defect formation are provided in the supplementary material (Notes S1 and S2 in Supporting information). At Te-rich, the availability of Cd atoms is reduced by the excess Te atoms, which lowers the formation energy of acceptor-type defects and enhances p-type conductivity. As a result, acceptor-type defects are more easily formed in a Te-rich environment, while donor-type defects have higher formation energies in a Cd-rich environment.

At Cd-rich, the formation energies of vacancy defects such as V_{Se}^{+2} and V_{Te}^{+2} are relatively low, indicating that these defects are more easily ionized and provide electrons, thereby promoting

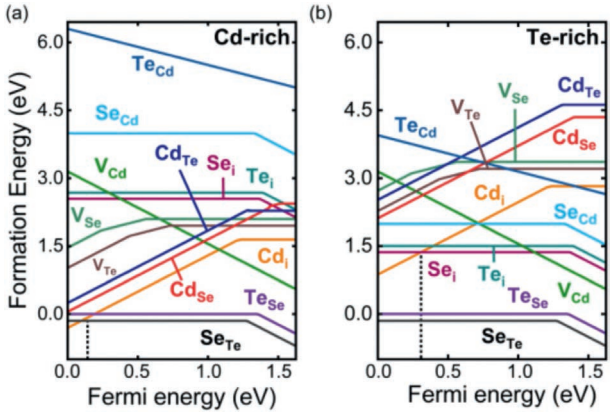


Fig. 3. The calculated formation energy of intrinsic defects in CTS as a function of the Fermi level under (a) Cd-rich (point A) and (b) Te-rich (point C) conditions. The slope of each line corresponds to the charge state of the defect: a positive slope indicates a donor-type defect that becomes more stable when ionized (*e.g.*, $q = +1$, $+2$), while a negative slope indicates an acceptor-type defect (*e.g.*, $q = -1$, -2). The charge states shown are consistent with those used in the main text and Fig. 2.

n-type conductivity. The vacancies of Se and Te are filled by excess Cd atoms, further reducing the formation energies of these defects and enhancing the donor effect (Fig. 3a). In contrast, the formation energies of Se_i^{2-} and Te_i^{2-} defects are lower at Te-rich environment, which suggests that they function as acceptor-type defects, efficiently capturing electrons and promoting p-type conductivity (Fig. 3b). Additionally, the low formation energies of Se_{Te}^{2-} and Te_{Cd}^{2-} defects in both Cd-rich and Te-rich environments suggest that these defects readily form under various chemical conditions, which is attributed to the chemical similarity between Se and Te. The similar atomic radii and valence electron structures of Se and Te lower the substitute energy in the lattice. Their strong lattice adaptability minimizes local distortions, thus reducing the formation energy of defects.

In semiconductor materials, the presence of defects plays a crucial role in carrier recombination behavior, directly influencing the carrier transport and optoelectronic properties of the material. In the investigation of carrier lifetime, we concentrate on the Se_{Cd}, Te_{Cd}, V_{Se}, Se_{Te} and Te_{Se} defect systems. These defects are selected for their ability to effectively widen the bandgap, suppress mid-gap defect state formation, and reduce non-radiative recombination pathways [32], demonstrating significant potential to enhance carrier lifetime (Fig. S1 in Supporting information). All defect configurations are modeled in their neutral charge states to ensure consistency in the evaluation of intrinsic recombination mechanisms. To further understand the impact of these defects on carrier recombination mechanisms, Hefei-NAMD-based computational framework is adopted to analyze their specific roles in the carrier recombination process, revealing the energy level changes induced by defects and the mechanisms governing carrier transitions between different defect states [42].

Based on MD simulations, the systems are heated to 300 K. During the heating process, anharmonic effects exert significant physical influence, particularly at higher temperatures, where phonon excitation and lattice vibrations play a crucial role in carrier behavior. Fig. 4 illustrates the temporal evolution of CBM, VBM, and defect energy levels at 300 K. By monitoring these energy levels, the strength of electron-phonon coupling can be directly observed, mainly reflected in the amplitude of energy level oscillations. As

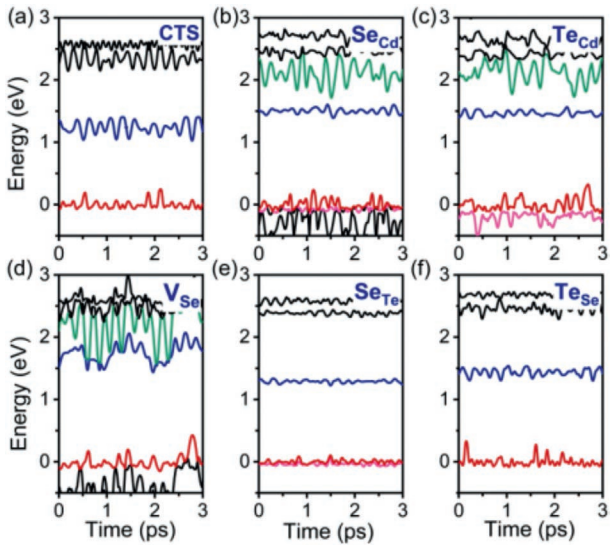


Fig. 4. The energy evolution of Kohn-Sham (KS) states in pristine CTS and defective systems. (a) Represents pristine CTS, (b) Se_{Cd}, (c) Te_{Cd}, (d) V_{Se}, (e) Se_{Te} and (f) Te_{Se}. The energy reference is set at the VBM of the initial configuration, with the red line representing the VBM, the blue line representing the CBM, and the magenta and green lines indicating defect levels near the VBM and CBM.

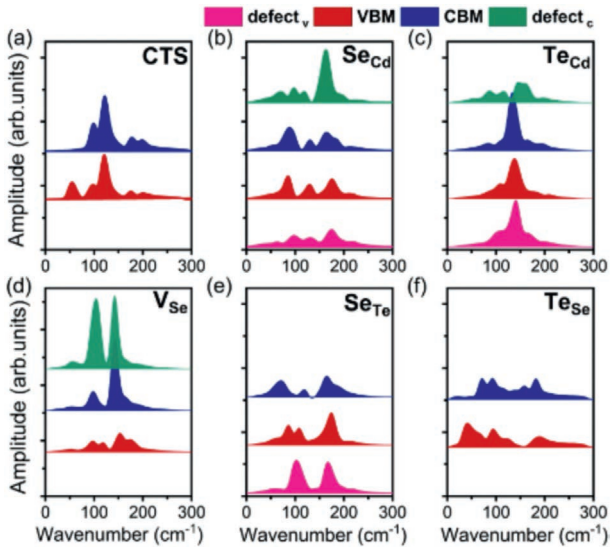


Fig. 5. FT spectra illustrating the frequency response of the VBM, CBM and defect states for pristine CTS and systems with defects, including (a) pristine CTS, (b) Se_{Cd}, (c) Te_{Cd}, (d) V_{Se}, (e) Se_{Te} and (f) Te_{Se}. The spectra capture the characteristic vibrational modes associated with each system's electronic states. For simplicity, defect states near the VBM are designated as *defect*$_v$, while those near the CBM are labeled as *defect*$_c$.

shown in Figs. 4b-f, except for the Te_{Se} defect, defect energy levels are introduced near the CBM or VBM by the other four defect systems (Se_{Cd}, Te_{Cd}, V_{Se}, Se_{Te}). The introduction of the defect energy levels alters the material's band structure, particularly for the Te_{Se} defect, which induces charge rearrangement, significantly altering the local charge distribution and increasing the density of electronic states near the band edges. In the pristine CTS system, the VBM and CBM exhibit significant time-dependent oscillations with an amplitude of approximately 0.3 eV. The oscillations suggest that the energy level positions fluctuate periodically due to temperature effects and electron-phonon interactions. The modulation effect of defect states is particularly evident in the Se_{Cd}, Te_{Cd} and V_{Se} systems during the molecular dynamics simulations, where the defects significantly influence dynamic changes in carrier energy levels by modifying the local electronic environment.

The primary phonon frequencies associated with electronic state coupling are characterized by Fourier transform (FT) spectra, as shown in Fig. 5. Across all systems, the primary phonon modes appear below 200 cm^{-1} in the low-frequency region, concentrated in the low-frequency region, which indicates weak phonon scattering and contributes to longer carrier recombination lifetime. In the pristine CTS system (Fig. 5a), the main phonon peaks occur at 53, 98 and 135 cm^{-1}. The 53 cm^{-1} vibrational mode couples with the VBM, the 98 cm^{-1} vibrational mode couples with both the CBM and the VBM, and the 135 cm^{-1} mode similarly shows this dual coupling characteristic. The interaction between the conduction and valence bands is enhanced by this dual coupling, which is crucial for carrier transitions and recombination dynamics. Furthermore, the phonon spectrum and phonon density of states (Phon-DOS) of CTS are calculated using density functional perturbation theory (DFPT) (Fig. S2 in Supporting information). Prominent peaks are observed in the Phon-DOS at 53, 98 and 135 cm^{-1}, aligning closely with the vibrational modes derived from Fourier transform calculations. Moreover, comparison with the Phon-DOS indicates that increasing temperature enhances anharmonic effects, leading to amplified vibrational amplitudes at these frequencies [43].

Following the introduction of the Se_{Cd} defect, a significant enhancement of the vibrational mode near 152 cm^{-1} is observed, accompanied by an increased amplitude (Fig. 5b), with strong

coupling to both defect states and band-edge states. This implies that local vibrations are induced by the defect, thus enhancing the electron-phonon interaction between the defect and the valence band. In the Te_{Cd} defect system, a significant enhancement of the vibrational mode at 135 cm^{-1} is observed, along with a strengthened coupling between the CBM and VBM. The enhancement is primarily attributed to the local lattice distortion induced by the defect (Fig. 5c). In contrast, in Se_{Te} and Te_{Se} defect systems, the emergence of new high-frequency phonon modes is observed, with these modes primarily manifesting as local vibrations (Figs. 5e and f). Although they influence the local electronic structure, their weak coupling with the band-edge states weakens the electron-phonon interaction. Furthermore, compared to the Se_{Cd} and Te_{Cd} defect systems, the low-frequency phonon modes in the Se_{Te} and Te_{Se} systems are less pronounced, indicating another potential mechanism for the effective suppression of non-radiative carrier recombination.

Non-adiabatic electron–hole (e–h) recombination refers to the relaxation of an excited-state electron from the conduction band minimum (CBM) to the valence band maximum (VBM). When defect states are present, the Shockley–Read–Hall (SRH) recombination model defines two main pathways: one involves direct recombination from the CBM to the VBM, and the other involves the electron being captured by a defect state, undergoing energy-level transitions, and eventually recombining with a hole [44]. DOS analysis shows that the defect systems studied here do not introduce significant defect states within the band gap (Fig. S1). Therefore, the recombination of electrons primarily occurs *via* the direct path. In the pristine CTS system, the carrier recombination time is 149.71 ns, which consists of existing experimental results, validating the reliability and accuracy of the model (Fig. 6a) [45,46]. In Se_{Cd}, Te_{Cd} and V_{Se} defect systems, the recombination times are shortened to 9.44, 30.95, and 80.03 ns, respectively (Figs. 6b-d), indicating that the introduction of defects accelerates the carrier recombination process. However, in the Se_{Te} and Te_{Se} defect systems (Figs. 6e and f), the recombination times significantly increase to 198.04 ns and 239.5 ns, respectively. Previous analysis has shown that the formation energies of Se_{Te} and Te_{Se} defects are the lowest in the CTS system, particularly under Cd-rich and Te-rich growth conditions, indicating that these defects are more likely to form during the growth of the CTS system. The findings provide essential theoretical guidance for the optimization and practical application of the CTS system. Specifically, Se_{Te} and Te_{Se} defect systems may significantly contribute to improving device performance.

The degree of coupling between two electronic states is described by the NAC. A larger NAC value indicates stronger coupling, which generally leads to an increased probability of electron transitions between these states, thereby accelerating the electron

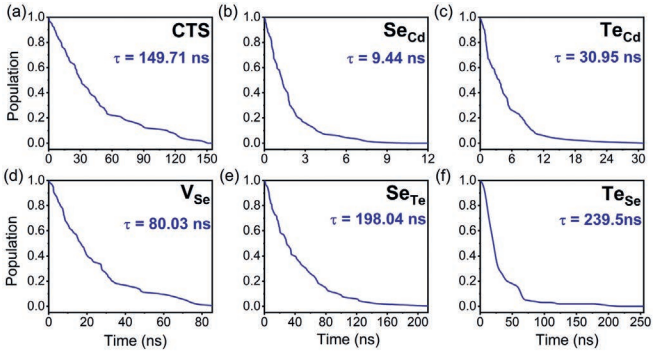


Fig. 6. *e–h* recombination dynamics illustrated by the time-dependent electron population on the CBM for pristine CZT and defective systems: (a) pristine CTS, (b) Se_{Cd}, (c) $Te_{Cd,}$ (d) V_{Se}, (e) Se_{Te} and (f) Te_{Se}.

Table 1
Average absolute NAC values (meV) and DT (fs) among the VBM, and the CBM for pristine CTS and defective systems.

Parameter	CTS	Se_{Te}	Te_{Se}	V_{Se}	Se_{Cd}	Te_{Cd}
NAC (meV)	8.8×10^{-4}	5.2×10^{-4}	4.3×10^{-4}	0.003	0.065	0.026
DT (fs)	4.42	4.29	4.04	6.28	10.8	7.05

relaxation process. In NAMD simulations, the lifetime of excited-state carriers is governed by NAC and decoherence time (DT), both of which are closely related to phonon excitation and electron-phonon coupling. The increased NAC values and longer DT between the CBM and VBM are pivotal in facilitating the dynamics of electron-hole recombination. Table 1 summarizes the NAC values and DT between the CBM and VBM, along with the coupling between defects and band edges. In Se_{Cd} and Te_{Cd} defect systems, the NAC values between the CBM and VBM are 0.065 and 0.026 meV, with corresponding DTs of 10.76 and 7.05 fs. The higher NAC values and longer DT promote rapid carrier transitions between energy levels, accelerating the electron-hole recombination process and further increasing the recombination rate. In contrast, the NAC values in Se_{Te} and Te_{Se} systems are much lower by at least two orders of magnitude, with values of 5.2×10^{-4} and 4.3×10^{-4} meV, respectively. Their DTs are also shorter, at 4.29 and 4.04 fs, respectively. The electron-hole recombination process appears to be inhibited by the lower NAC values and shorter DTs. Specifically, the carrier recombination times in the Se_{Te} and Te_{Se} systems are about 32- and 39.4-fold greater than that of the Se_{Cd} system, respectively. The result underscores the pivotal role of NAC in recombination dynamics, illustrating that optimizing NAC values can effectively regulate the recombination rate and improve the material's opto-electronic properties.

To further investigate the factors regulating carrier recombination mechanisms, we focus on the impact of carrier concentration on the recombination process, revealing its significant role in recombination behavior. In the systems studied, recombination occurs between the CBM and the VBM. Therefore, the band-to-band recombination mechanism in the CTS system is discussed, with detailed calculations presented in Notes 3 (Supporting information).

With a fixed equilibrium carrier concentration n_0 (10^{15} cm^{-3}), as the initial non-equilibrium carrier concentration $\Delta n(0)$ increases from 10^{12} cm^{-3} to 10^{22} cm^{-3}, the recombination lifetime $\tau_{band\text{-}band}$ drastically decreases from the millisecond to the nanosecond scale (Fig. 7a). Other n_0 values also show the same trend, indicating that higher initial non-equilibrium carrier concentration accelerates the recombination process. Furthermore, for a fixed $\Delta n(0)$, as n_0 increases, $\tau_{band\text{-}band}$ exhibits two trends (Fig. 7b). Specifically, when n_0 (or p_0) is much smaller than $\Delta n(0)$, $\tau_{band\text{-}band}$ remains nearly constant, suggesting that $\Delta n(0)$ primarily governs the change in the recombination rate. This applies to most intrinsic semiconductors, where n_0 and p_0 are typically low (for intrinsic CTS, n_0 and p_0 are approximately 1.404×10^6 cm^{-3}), significantly lower than the value of $\Delta n(0)$ (2.307×10^{20} cm^{-3}). In the case of high defect density (2.307×10^{20} cm^{-3} in this work), n-type defects correspond to a high equilibrium electron concentration, while p-type defects correspond to a high equilibrium hole concentration. The system's n_0 and p_0 become comparable to $\Delta n(0)$, as shown by the shift in the line in Fig. 7a and the reduction in lifetime at both ends of Fig. 7b. These results suggest that the influence of n_0 and p_0 on the recombination process intensifies at higher concentrations [47].

The time decay behavior of non-equilibrium carrier concentration is investigated under various initial concentration conditions (Figs. 7c and d), With an initial concentration $\Delta n(0)$ of 2.307×10^{20} cm^{-3}, decreases rapidly to 1/e of its initial value within nanoseconds. A further reduction in $\Delta n(0)$ to 2.307×10^{15} cm^{-3} results in an increased decay time, extending

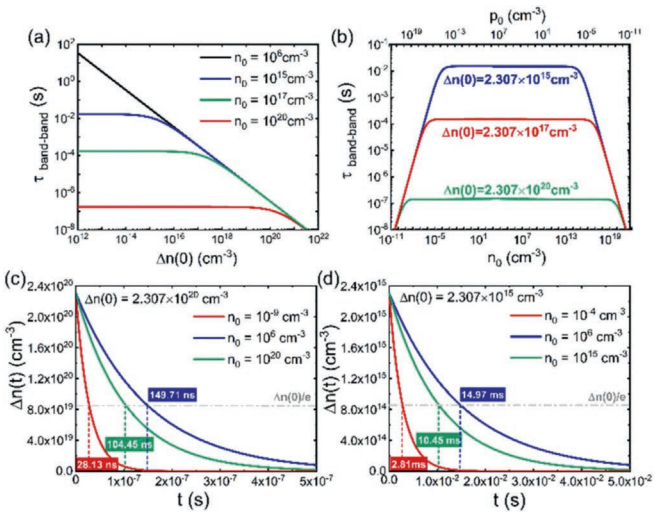


Fig. 7. The calculated dependence of $\tau_{\text{band-band}}$ of CTS system. (a) $\tau_{\text{band-band}}$ as a function of the initial non-equilibrium carrier concentration $\Delta n(0)$ for different equilibrium carrier concentration $n_0(p_0)$. (b) $\tau_{\text{band-band}}$ as a function of $n_0(p_0)$ for given values of $\Delta n(0)$. The time evolution of carrier concentration $\Delta n(t)$ of CTS system. (c) The time evolution of carrier concentration $\Delta n(t)$ for $\Delta n(0) = 2.307\times10^{20}$ cm^{-3}, with three different $n_0(p_0)$ values. (d) The time evolution of $\Delta n(t)$ for $= 2.307\times10^{15}$ cm^{-3}, again with three different $n_0(p_0)$ values.

to the millisecond range. Furthermore, in n-type defects, when n_0 is very high, the simulated decay of $\Delta n(t)$ significantly accelerates, and a similar trend is observed for the high value of p_0 corresponding to p-type defects. Therefore, by precisely controlling carrier concentration, both the recombination rate can be regulated, and the optoelectronic properties of the material can be optimized. In the design and application of optoelectronic devices, effective carrier concentration control can improve device efficiency, minimize energy loss, and prolong the device lifespan.

This study systematically investigates the electronic structure, formation energies, and transition levels of intrinsic defects in CTS materials using DFT and NAMD methods, offering new insights into the critical properties of excited-state carrier dynamics. The findings reveal that Te-rich conditions promote the formation of acceptor defects (*e.g.*, V_{Cd}^{2-} and Se_i^{2-}) enhancing p-type conductivity, whereas Cd-rich conditions favor the generation of donor defects (*e.g.*, V_{Se}^{+2} and V_{Te}^{+2}), improving n-type conductivity. Furthermore, Se_{Te} and Te_{Se} defects exhibit high thermodynamic stability due to their low formation energies, allowing them to form preferentially across diverse chemical environments, thereby offering significant potential for material performance optimization. Further analysis reveals that defects like Se_{Cd} and Te_{Cd} enhance electron-phonon coupling, significantly shortening carrier recombination times, while Se_{Te} and Te_{Se} defects suppress the NAC through weaker coupling, extending recombination times. FT analysis highlights that the phonon modes of different defect systems are mainly concentrated in the low-frequency region (below 200 cm^{-1}), with the weak electron-phonon coupling in Se_{Te} and Te_{Se} defects further optimizing carrier dynamics. Finally, non-equilibrium carrier concentration significantly affects recombination processes. At higher concentrations, recombination times shorten significantly, highlighting the importance of defect engineering in controlling recombination dynamics. Se_{Te} and Te_{Se} defects show significant potential for improving optoelectronic performance, providing a theoretical basis for optimizing CTS material performance and practical applications.

CRediT authorship contribution statement

Hongqin Chu: Writing – original draft, Formal analysis. **Liyang Li:** Investigation. **Fan Yang:** Visualization, Conceptualization. **Shujuan Li:** Writing – review & editing, Conceptualization. **Jiayao Wang:** Formal analysis. **Shulai Lei:** Writing – review & editing, Supervision, Software. **Jinbo Sun:** Investigation. **Ke Xu:** Funding acquisition. **Xinyue Xiong:** Visualization, Validation. **Zhenpeng Hu:** Writing – review & editing, Supervision, Funding acquisition.

Declaration of competing interest

The authors declare that they have no known competing financial interests or personal relationships that could have appeared to influence the work reported in this paper.

Acknowledgments

This work was supported by the National Key R&D Program of China (No. 2022YFB3503901), the National Natural Science Foundation of China (Nos. 12134019, 12175110, 21773124, 11775120 and 11535010), the Fundamental Research Funds for the Central Universities (Nankai University, Nos. 010-63243091, 63233001, 63221346), Natural Science Foundation of Hubei Province (No. 2022CFC030) and Hubei University of Arts and Science (No. 2020kypytd002). This work was also supported by the Supercomputing Center of Nankai University (NKSC).

Supplementary materials

Supplementary material associated with this article can be found, in the online version, at doi:10.1016/j.cclet.2025.111490.

References

[1] T.A.M. Fiducia, B.G. Mendis, K. Li, et al., Nat. Energy 4 (2019) 504–511.
[2] P. Capper, E.S. O'Keefe, C. Maxey, et al., J. Cryst. Growth 161 (1996) 104–118.
[3] K.H. Kim, J.K. Hong, S.U. Kim, J. Cryst. Growth 310 (2008) 91–95.
[4] U.N. Roy, A.E. Bolotnikov, G.S. Camarda, et al., Proc. SPIE 9213 (2014) 92130F.
[5] I. Hähnert, M. Mühlberg, H. Berger, et al., J. Cryst. Growth 142 (1994) 310–314.
[6] U.N. Roy, A.E. Bolotnikov, G.S. Camarda, et al., J. Cryst. Growth 386 (2014) 43–46.
[7] U.N. Roy, A.E. Bolotnikov, G.S. Camarda, et al., APL Mater. 3 (2015) 021101.
[8] U.N. Roy, A.E. Bolotnikov, G.S. Camarda, et al., J. Cryst. Growth 411 (2015) 34–37.
[9] M. Fiederle, D. Ebling, C. Eiche, et al., J. Cryst. Growth 138 (1994) 529–533.
[10] A.H. Munshi, J. Kephart, A. Abbas, J. Raguse, et al., IEEE J. Photovolt. 8 (2018) 310–314.
[11] R. Gul, U.N. Roy, A.E. Bolotnikov, et al., APL Mater. 3 (2015) 041101.
[12] N.X. Ca, N.T. Hien, P.V. Do, et al., RSC Adv. 13 (2023) 36455–36466.
[13] C. Li, X. Hao, J. Zhang, et al., Conf. Rec. IEEE Photovolt. Spec. Conf. 2020 (2020) 2649–2651.
[14] A. Nagaoka, K. Nishioka, K. Yoshino, et al., J. Electron. Mater. 49 (2020) 6971–6976.
[15] U.N. Roy, A.E. Bolotnikov, G.S. Camarda, et al., J. Cryst. Growth 389 (2014) 99–102.
[16] G. Kresse, J. Furthmüller, Comput. Mater. Sci. 6 (1996) 15–50.
[17] G. Kresse, J. Furthmüller, Phys. Rev. B 54 (1996) 11169–11186.
[18] S.H. Wei, S.B. Zhang, Phys. Rev. B 66 (2002) 155211.
[19] J.Y. Noh, H. Kim, Y.S. Kim, Phys. Rev. B 89 (2014) 205417.
[20] V. Wang, Y. Kawazoe, W.T. Geng, Phys. Rev. B 91 (2015) 045433.
[21] X. Xiang, Y. Tong, A. Gehrke, et al., Phys. Rev. Mater. 8 (2024) 084602.
[22] W.J. Yin, S.H. Wei, M.M. Al-Jassim, et al., Phys. Rev. B 83 (2011) 155102.
[23] C. Persson, Y.J. Zhao, S. Lany, et al., Phys. Rev. B 72 (2005) 035211.
[24] Q. Zheng, W. Chu, C. Zhao, et al., WIREs Comput. Mol. Sci. 9 (2019) e1411.
[25] C.F. Craig, W.R. Duncan, O.V. Prezhdo, Phys. Rev. Lett. 95 (2005) 163001.
[26] W. Chu, Q. Zheng, O.V. Prezhdo, et al., Sci. Adv. 6 (2020) eaaw7453.
[27] L. Zhang, W. Chu, Q. Zheng, et al., Phys. Chem. Chem. Phys. 24 (2022) 4743–4750.
[28] L. Zhang, W. Chu, Q. Zheng, et al., J. Phys. Chem. Lett. 10 (2019) 6151–6158.
[29] W. Chu, W.A. Saidi, J. Zhao, et al., Angew. Chem. Int. Ed. 59 (2020) 6435–6441.
[30] S. Na-Phattalung, M.F. Smith, K. Kim, et al., Phys. Rev. B 73 (2006) 125205.
[31] J. Buckeridge, T.D. Veal, C.R.A. Catlow, D.O. Scanlon, Phys. Rev. B 100 (2019) 035207.
[32] H. Guo, W. Chu, Q. Zheng, et al., J. Phys. Chem. Lett. 11 (2020) 4662–4667.
[33] J. Paier, M. Marsman, K. Hummer, et al., J. Chem. Phys. 124 (2006) 154709.
[34] A.V. Krukau, O.A. Vydrov, A.F. Izmaylov, G.E. Scuseria, J. Chem. Phys. 125 (2006) 224106.
[35] D. Joubert, Phys. Rev. B 59 (1999) 1758–1775.
[36] M. Schenk, C. Silber, J. Mater. Sci. Mater. Electron. 9 (1998) 295–300.
[37] K. Okhotnikov, T. Charpentier, S. Cadars, J. Cheminform. 8 (2016) 17.

[38] L. Zhang, Q. Zheng, Y. Xie, et al., Nano Lett. 18 (2018) 1592–1599.
[39] Q. Zheng, W.A. Saidi, Y. Xie, et al., Nano Lett. 17 (2017) 6435–6442.
[40] A.V. Akimov, O.V. Prezhdo, J. Chem. Theory Comput. 10 (2014) 789–804.
[41] E. Cassette, S. Pedetti, B. Mahler, et al., Phys. Chem. Chem. Phys. 19 (2017) 8373–8379.
[42] Z.F. Zheng, X. Jiang, W.B. Chu, et al., Acta Phys. Sin. 70 (2021) 177101.
[43] Z. Wu, Phys. Rev. B 81 (2010) 172301.
[44] A. Alkauskas, C.E. Dreyer, J.L. Lyons, C.G. Van de Walle, Phys. Rev. B 93 (2016) 201304(R).
[45] N.X. Ca, N.T. Hien, P.N. Loan, et al., J. Electron. Mater. 48 (2019) 2593–2599.
[46] H.T. Van, N.D. Vinh, P.M. Tan, et al., Opt. Mater. 97 (2019) 109392.
[47] S. Wang, M. Huang, Y.N. Wu, et al., Nat. Comput. Sci. 2 (2022) 486–493.